LRP 691/01 March 2001

Full Absorption of 3rd Harmonic ECH in TCV Target Plasmas Produced by 2nd Harmonic ECH and ECCD

S. Alberti, T.P. Goodman, M.A. Henderson, A. Manini,
J.-M. Moret, P. Gomez, P. Blanchard, S. Coda, O. Sauter
and the TCV Team

Submitted for publication to
Physical Review Letters

ISSN 0458-5895

Full Absorption of 3rd Harmonic ECH in TCV Target Plasmas produced by 2nd Harmonic ECH and ECCD

S. Alberti, T.P. Goodman, M.A. Henderson, A. Manini, J.-M. Moret, P. Gomez, P. Blanchard, S. Coda, O. Sauter, C. Angioni, K. Appert, R. Behn, P. Bosshard, R. Chavan, I. Condrea, A. Degeling, B.P. Duval, D. Fasel, J.-Y. Favez, I. Furno, F. Hofmann, P. Lavanchy, J.B. Lister, X. Llobet, Z.A. Pietrzyk, A. Gorgerat, P. Gorgerat, J.-P. Hogge, P.-F. Isoz, B. Joye, J.-C. Magnin, B. Marlétaz, P. Marmillod, Y. Martin, A. Martynov, J.-M. Mayor, J. Mlynar, P. Nikkola, P.J. Paris, A. Perez, Y. Peysson[1], R.A. Pitts, A. Pochelon, H. Reimerdes, J. H. Rommers, E. Scavino, G. Tonetti, M.Q. Tran and H. Weisen

Centre de Recherches en Physique des Plasmas (CRPP-PPB)

Association EURATOM - Confédération Suisse

Ecole Polytechnique Fédérale de Lausanne, CH-1015 Lausanne, Switzerland

[1]*Association Euratom-CEA sur la fusion, DRFC, CEA-Cadarache, France*

(March 15, 2001)

Abstract

An experimental study of the extraordinary mode (X-mode) absorption at the third electron cyclotron (EC) harmonic frequency (118GHz) has been performed on the TCV Tokamak in plasmas preheated by X-mode at the second harmonic (82.7GHz). Full single-pass absorption of the 470kW of injected X3 power was measured with as little as 350kW of X2-CO-ECCD preheating. The measured absorption exceeds that predicted by the linear ray tracing code TORAY by more than a factor of 2 for the CO-ECCD case. Experimental evidence indicates that a large fraction of the X3 power is absorbed by

electrons in an energetic tail created by the X2-ECCD preheating.

52.35.Hr, 52.50.Sw, 52.25.Os

The use of electron cyclotron (EC) waves in magnetically confined plasmas such as tokamaks or stellerators has demonstrated in the past years the applications of EC waves in fusion relevant plasmas in terms of highly efficient localized heating and current drive [1,2], MHD control [3] and formation of improved core electron confinement [4]. However, in overdense plasmas ($\omega_{pe}^2/\Omega_{ce}^2 >> 1$, ω_{pe} and Ω_{ce} being the electron plasma frequency and electron cyclotron frequency, respectively) EC heating (ECH) is restricted for wave frequencies ω near the fundamental cyclotron frequency and second harmonic because the wave is reflected by a cutoff layer before it can reach the resonance. Options for overcoming the density limit are the O-X-B mode conversion [5] or, alternatively, heating at the 3^{rd} harmonic in X-mode.

For a Maxwellian distribution function and a harmonic number $n \geq 2$ the optical thickness τ_{Xn} of the X-mode is proportional to the small term $(k_B T_e/m_e c^2)^{n-1}$ (in case of O-mode with quasi perpendicular injection the optical thickness τ_{On} is proportional to $(k_B T_e/m_e c^2)^n$ with $n \geq 1$); consequently the absorption of the X-mode at the third harmonic is significantly weaker than at the second harmonic. However, in presence of EC current drive (ECCD) [1,6] or current drive by a lower hybrid wave [7,8], the electron distribution function becomes non-Maxwellian and affects not only the wave damping rate but also the location of energy deposition and the current drive efficiency of the EC wave [9,10]. In this Letter the first experimental evidence of the role of suprathermal electrons on the absorption of the 3rd harmonic X-mode is demonstrated.

For the first time in the TCV Tokamak, plasmas have been heated using the third harmonic EC X-mode (X3). The first of three 0.5MW gyrotrons operating at a frequency of 118 GHz [11] has been used. One of the motivations for X3 ECH in TCV is the possibility of heating at densities which are inaccessible with the existing X2 ECH system (82.7 GHz, $P_{X2} = 3$ MW). The final configuration of the X3 heating ($P_{X3} = 1.5$ MW), the launching geometry will be vertical (top launch) such that the RF beam $\vec{k}$ vector will have a very shallow incidence angle on the 3rd harmonic resonant layer. Low power transmission measurements in this launching configuration have been performed by Segui et al. [12] on

a target plasma with ohmic heating only. Comparison with linear ray tracing/absorption calculations, assuming a Maxwellian distribution function, have been shown to be consistent with the measurements.

In the experiment reported here, the X3 wave was launched from the low field side via one of the upper lateral launching antenna normally used for X2 heating [13]. In this launching scheme the RF beam $\vec{k}$ vector has a large incidence angle on the resonance layer and therefore is favourable for interaction with a wide electron energy spectrum. These experiments were aimed at establishing the importance of plasma conditions on the absorption of X3 ECH power. For this purpose the plasmas were preheated with different power levels of X2 ECH and ECCD.

The target plasmas used in these experiments have the parameters R=0.88m, a=0.25m, elongation $\kappa = 1.31$, $B_T = 1.42T$, $n_e(0) = 2.5 \times 10^{19} m^{-3}$. The cold resonances corresponding to the X2 and X3 frequencies are spatially separated by approximately 50mm, and, in the target plasma studied here, they are symmetric with respect to the plasma center; the X3 cold resonance being on the low field side.

The launching geometry, as well as time traces of the relevant plasma parameters, are shown in Fig. 1. The top trace shows the time sequences for the 2nd and 3rd harmonic heating. For all launching configurations the X2 was kept at constant power from 0.3s to 1.3s whereas the X3 power was applied from 0.5s to 1.2s and included a phase with 100% modulation at 237Hz between 0.8s and 1s. The large fluctuations on the central electron temperature measured by Thomson scattering are related to the sawtoothing character of the plasma and the 50ms interval between Thomson measurements, the low temperature values being correlated with sawtooth crashes. The total stored energy variation was measured during the modulated portion of the X3 RF pulse using a diamagnetic loop (DML). The modulation frequency $f_m = 237Hz$ was chosen such that $1/2\pi f_m < \tau_e \approx 5ms$, where τ_e is the electron energy confinement time. While the X3 power (0.47MW) and launching antenna, aimed at the plasma centre, were kept constant in this series of experiments, different X2 conditions were investigated including variations of the toroidal launch angle, the power

deposition radius and the total X2 power.

All absorption measurements have been performed with the DML diagnostic in the modulated phase of the X3 power injection which provides an absolute measurement of the absorbed rf power. Figure 2 shows the X3 absorbed power fraction versus X2 preheat power for three X2 launching angles corresponding to central CO-ECCD ($\phi = 20^o$), ECH ($\phi = 0^o$) and CNT-ECCD ($\phi = -20^o$) (all toroidal angles are defined at the absorption location, $\cos(\phi + \pi/2) = \frac{\vec{k}.\vec{B}}{|\vec{k}||\vec{B}|}$ and $\vec{B}$ is the equilibrium magnetic field). For CO-ECCD target plasmas, within the experimental error bars, 100% absorption is obtained. A polarization scan of the X3 rf-beam as well as a poloidal scan of the launching angle (from central to off-axis, $r/a > 0.5$) has demonstrated that essentially single-pass absorption is measured.

The X3 absorbed fraction depends in an asymmetric way on the toroidal injection angle of the X2 launch (Fig. 3). The measured X3 absorption (circles) is highest in a target plasma with X2 having a toroidal angle of $\phi = 20^o$, corresponding to CO-ECCD. The calculated absorption with the linear ray tracing code TORAY [14] (squares) assumes an isotropic Maxwellian distribution function. For the largest toroidal angle in CO-ECCD ($\phi = 52^o$), significant refraction of the X2 wave is occurring with a resulting X2 absorption of only 38% (TORAY). For all other toroidal angles, full single-pass absorption of X2 is predicted. For this same toroidal angle scan, the variation of the plasma bulk parameters measured by Thomson scattering such as peak electron temperature and density and the behaviour of the suprathermal tail measured by the hard x-ray camera are shown in Fig. 4. The strong asymmetry in the measured absorption observed in Fig. 3 can also be seen on the bulk plasma parameters during the X3 heating. Note that this is reflected in some degree of asymmetry on the TORAY results (Fig. 3) but is still not sufficient to account for high absorption.

Calculations of the theoretical absorption with the ray tracing code TORAY, assuming an isotropic, Maxwellian velocity distribution, are in fair agreement with the experimental results corresponding to ECH ($\phi = 0^o$) preheating. This observation is also in agreement with X3 absorption measurements by Pachtman et al. [15]. However, the measured X3

absorption exceeds that predicted by TORAY by a factor of up to 2 for the CNT- and CO-ECCD cases. A likely explanation of the discrepancy is that a large fraction of the X3 power is absorbed by energetic tail electrons created by X2 ECCD. The presence of these tails is confirmed by the measurement of photon spectra using an energy resolving hard x-ray camera (Figs. 1 and 4c)) and a high field side ECE radiometer (Fig. 5).

The photon energy spectrum measured with the hard x-ray camera can be fitted with a bi-maxwellian distribution function. The tail photon temperature T_{pht} strongly depends on the toroidal injection angle and during the X3 heating T_{pht} varies between 12keV at $\phi = 0^o$ to 30keV at $\phi = 40^o$. An indication of the tail electron density is given by the integrated photon emissivity associated with the tail of the fitted bi-maxwellian distribution. In Fig. 4c) the integrated tail photon emissivity is shown against the toroidal angle for both the X2 preheating phase and the X3 heating. The strong correlation observed between the absorbed fraction curve of Fig. 3 and the tail emissivity is an additional evidence of the role of suprathermal electrons in the enhanced absorption of X3.

Similar to the hard x-ray camera results, the high-field side ECE radiometer detects suprathermal radiation levels several times larger than the thermal level in the presence of ECCD. The radiometer time traces in Fig. 5 show that during the X2 preheating ($0.3s < t < 0.5s$), no suprathermal electrons are generated for the quasi-ECH case (top), since the signals are consistent with Thomson. For the CO-ECCD case a significant deviation from Thomson is observed, which indicates the presence of a suprathermal electron tail. By comparing the two radiometer channels in the two cases (quasi-ECH and CO-ECCD) one can deduce that the suprathermal electrons are spatially located between the normalized minor radii $r/a = 0$ and $r/a = 0.5$ since, for the off-axis channel ($R = 0.75m$), the deviation from Thomson is very weak during the entire plasma discharge. The photon counts and the ECE radiometer are consistent in showing a weaker generation of suprathermal electrons during the ECH preheating phase.

The strong dependence of the X3 absorbed fraction versus toroidal injection angle of the X2 wave, showing a resonant like behaviour around $\phi = 20^0$, can be qualitatively understood

by the following simplified 1D model illustrated in Fig. 6. In this figure, the x-axis is the distance from the X2 cold resonance in the direction of the low-field side. For the X3 wave with perpendicular incident angle (ECH) from the low field side, the single particle resonant energy (left y-axis) is indicated by the dash-dotted line. For the X2 wave incident from the low field side, depending on the toroidal incidence angle, the wave starts to interact with suprathermal electrons before it reaches the X2 cold resonance. For a given toroidal angle (right y-axis), the radial position where this occurs is shown by the dashed line on Fig. 6 and is given by the condition [2] $n\Omega_{ce}(r)/\omega_{X2} = \sqrt{1 - N_{||}^2}$, where $n = 2$, $\omega_{X2} = 2\pi f_{X2}$ ($f_{X2} =$ 82.7 GHz) and $N_{||} = \sin\phi$. The corresponding single particle resonant energy for the X2 wave at the radial position defined above is given by the equation $E_{spX2} \simeq (1/2)\sin^2\phi\, m_e c^2$ and is indicated on Fig. 6 by the solid line. The intersection between the single particle resonant energies for the X2 and X3 waves defines the radial position where both waves can interact at the same radial position with electrons of same kinetic energy. In the present configuration this situation corresponds to a toroidal angle close to 14^0, and for electron energies around 14-16 [keV] consistent with the measured suprathermal photon energy. The difference between the toroidal angle of 14^0 predicted by this simplified model and the measured angle of 20^0 can be explained by the fact that the maximum absorption for the X2 wave takes place on the high field side of the radial position defined above. This simplified 1D model does not explain the toroidal angle asymmetry observed in Fig. 3. However, geometric effects have been completely neglected, such as variation of $N_{||}$ along the rays due to toroidal curvature. Guided by this model, we are presently conducting a detailed analysis of the experimental data including 2D effects (refraction, temperature profiles, equilibrium magnetic field, etc.) accompanied by calculations of self-consistent distribution functions by means of a Fokker-Planck code. This work will be the subject of a future publication.

In summary, the first application of high power X3 heating on the TCV tokamak has been demonstrated. Absorption measurements are in agreement with TORAY calculations for ohmic and ECH heated plasmas with a maxwellian electron distribution function. Increased (full) single-pass absorption of the 3rd harmonic X-mode, beyond TORAY calculations, has

been measured with X2-ECCD preheated plasmas. Experimental evidence shows that the increased absorption is associated with the presence of a suprathermal tail in the electron distribution function.

This work was partly supported by the Swiss National Science Foundation. The hard x-ray camera is on loan from the Tore Supra group (CEA, Cadarache).

REFERENCES

[1] O. Sauter *et al.*, Phys. Rev. Lett. **84**,3322 (2000).

[2] V. Erckmann and U. Gasparino, Plasma Phys. Control. Fusion **36**, 1869 (1994).

[3] H. Zohm *et al.*, Nucl. Fusion **39**,577 (1999).

[4] Z.A. Pietrzyk *et al.*, *To be published in* Phys. Rev. Lett.

[5] J. Preinhalter *et al.*, J. Plasma Phys. **10**, 1 (1973); H.P. Laqua *et al.*, Phys. Rev. Lett. **78**,3467 (1997).

[6] K.L. Wong *et al.*, Phys. Rev. Lett. **85**,996 (2000).

[7] V. Pericoli-Ridolfini *et al.*, in *Proceedings of the 18th IAEA Fusion Energy Conference, Sorrento, 2000.*

[8] K. Kato and I.H. Hutchinson, Phys. Rev. Lett. **56**,340 (1986).

[9] K. Matsuda and J.Y. Hsu, Phys. Fluids B **3**, 414 (1991).

[10] G.E. Guest *et al.*, Nucl. Fusion **27**, 1245 (1987).

[11] S. Alberti *et al.*, Fus. Eng. Des. **53**,387 (2001).

[12] J.-L. Ségui *et al.*, Nucl. Fusion **36**, 1245 (1996).

[13] T.P. Goodman *et al.*, in *Proceedings of the 19th Symposium on Fusion Technology, Lisbon 1996*, edited by C. Varandas and F. Serra (North-Holland, Amsterdam, 1997), p.565.

[14] G.R. Smith *et al.*, in *Proceedings of the 9th Joint Workshop on ECE and ECRH, Borrego Springs, CA, 1995*, (World Scientific, Singapore, 1995), p.651.

[15] A. Pachtman *et al.*, Nucl. Fusion **27**, 1283 (1987).

FIGURES

FIG. 1. Launching geometry and typical time traces for the X2 and X3 ECH. For X2, the local toroidal angle at the absorption location is $\phi = 20^{o}$ (CO-ECCD). From top to bottom: RF power for X2 and X3, poloidal beta, loop voltage, soft x-ray signal (central chord), hard x-ray signal (central chord), Thomson scattering peak electron temperature and density (every 50ms) and line average density. RF power: $P_{X2} \approx P_{X3} = 0.47MW$. Plasma current: $I_p = 200kA$.

FIG. 2. Measured X3 absorption using the DML versus X2 preheat power for three different X2 launching configurations: CO-ECCD ($\phi = 20^{o}$), CNT-ECCD ($\phi = -20^{o}$) and ECH ($\phi = 0^{o}$). The 3rd harmonic injected power was kept constant at 0.47MW with central deposition and zero toroidal injection angle (ECH).

FIG. 3. Measured absorption with DML (circles) and calculated absorption with TORAY (squares) versus X2 injection angle. The X2 and X3 injected power are equal at 470 kW. The TORAY code assumes an isotropic Maxwellian distribution function.

FIG. 4. Peak central electron temperature (a) and density (b) (Thomson scattering) and total x-ray emissivity of the suprathermal tail (c) (Hard x-ray camera) versus toroidal angle. The X2 and X3 power are as in Fig. 3. The suprathermal tail emissivity is extrapolated from exponential fit to suprathermal hard x-ray spectrum, and is set to zero when it is too low to be separated from the thermal signal. The squares correspond to measurements during the X2 preheating phase(0.3-0.5s) while the circles are measured with the X3 power applied.

FIG. 5. Time traces of the high field-side ECE radiometer: quasi-ECH at $\phi = -6.5^{o}$ (top) and CO-ECCD at $\phi = 20^{o}$ (bottom). In both figures, two radiometer channels are shown: a on-axis view ($R = 0.88m$, black trace) and an off axis view (R= 0.75m, grey trace). All radiometer signals have been calibrated against the Thomson scattering diagnostic (circles) during the ohmic phase ($t < 0.3s$). $P_{X2} \approx P_{X3} = 0.47MW$.

FIG. 6. Single particle resonance energies (left y-axis, E_{sp}) for X2, E_{spX2} (solid line), and X3, E_{spX3} (dash-dotted line), waves versus radial distance from the X2 cold resonance going towards the low-field side. For an oblique incidence with toroidal angle ϕ, the dashed line indicates the radial position at which the X2 wave starts to interact with electrons having a kinetic energy E_{spX2}.

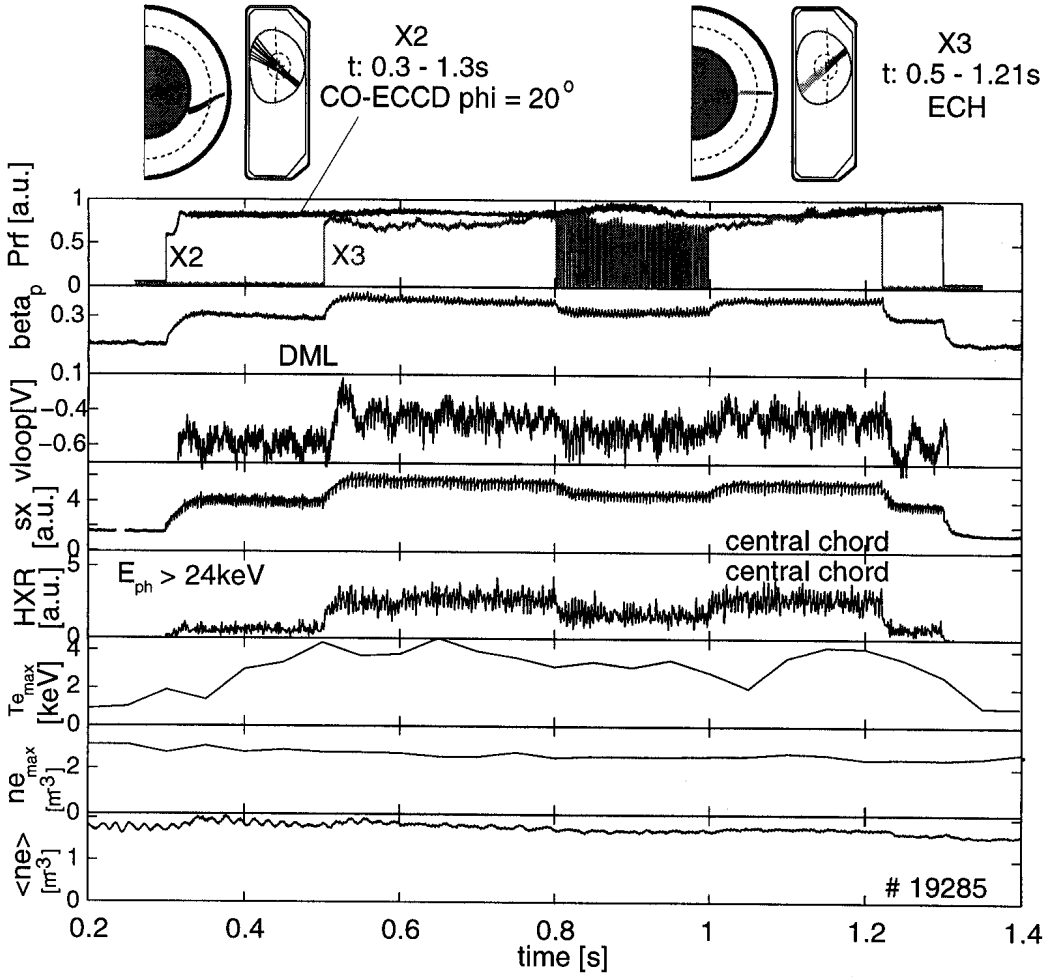

FIG. 1. Launching geometry and typical time traces for the X2 and X3 ECH. For X2, the local toroidal angle at the absorption location is $\phi = 20^o$ (CO-ECCD). From top to bottom: RF power for X2 and X3, poloidal beta, loop voltage, soft x-ray signal (central chord), hard x-ray signal (central chord), Thomson scattering peak electron temperature and density (every 50ms) and line average density. RF power: $P_{X2} \approx P_{X3} = 0.47MW$. Plasma current: $I_p = 200kA$.

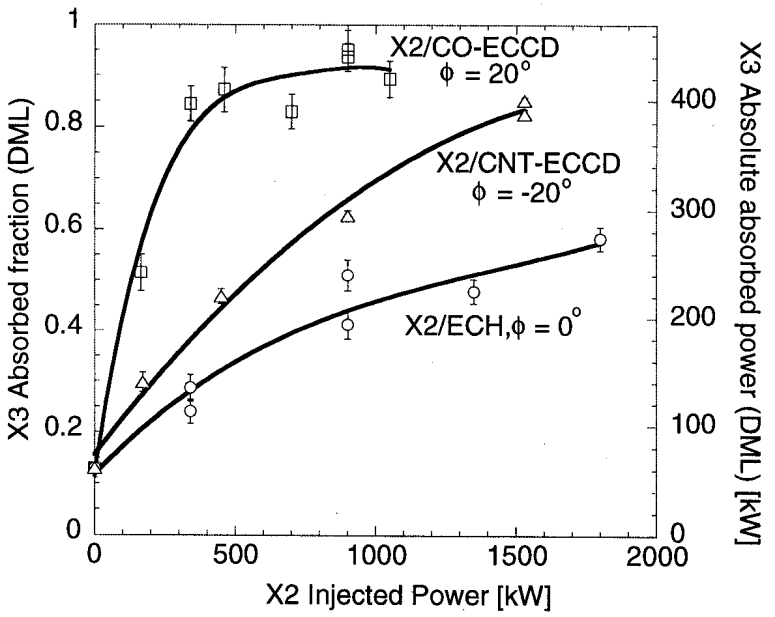

FIG. 2. Measured X3 absorption using the DML versus X2 preheat power for three different X2 launching configurations: CO-ECCD ($\phi = 20°$), CNT-ECCD ($\phi = -20°$) and ECH ($\phi = 0°$). The 3rd harmonic injected power was kept constant at 0.47MW with central deposition and zero toroidal injection angle (ECH).

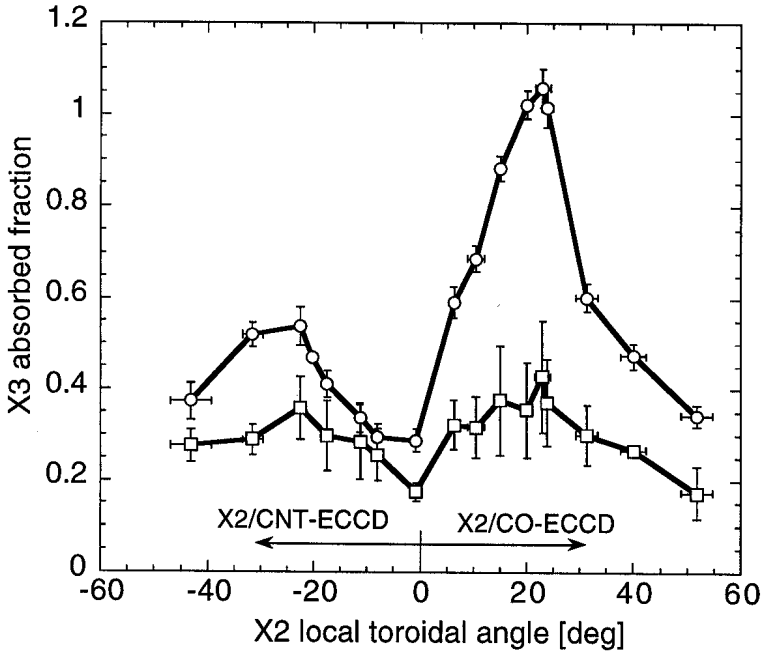

FIG. 3. Measured absorption with DML (circles) and calculated absorption with TORAY (squares) versus X2 injection angle. The X2 and X3 injected power are equal at 470 kW. The TORAY code assumes an isotropic Maxwellian distribution function.

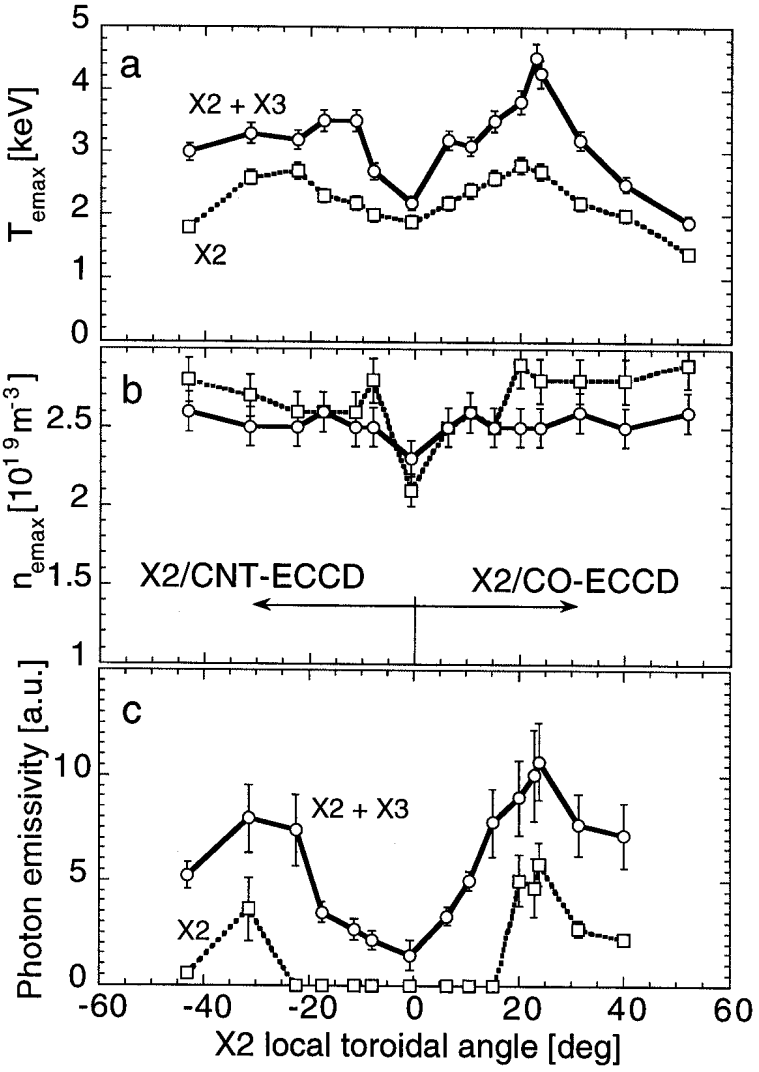

FIG. 4. Peak central electron temperature (a) and density (b) (Thomson scattering) and total x-ray emissivity of the suprathermal tail (c) (Hard x-ray camera) versus toroidal angle. The X2 and X3 power are as in Fig. 3. The suprathermal tail emissivity is extrapolated from exponential fit to suprathermal hard x-ray spectrum, and is set to zero when it is too low to be separated from the thermal signal. The squares correspond to measurements during the X2 preheating phase(0.3-0.5s) while the circles are measured with the X3 power applied.

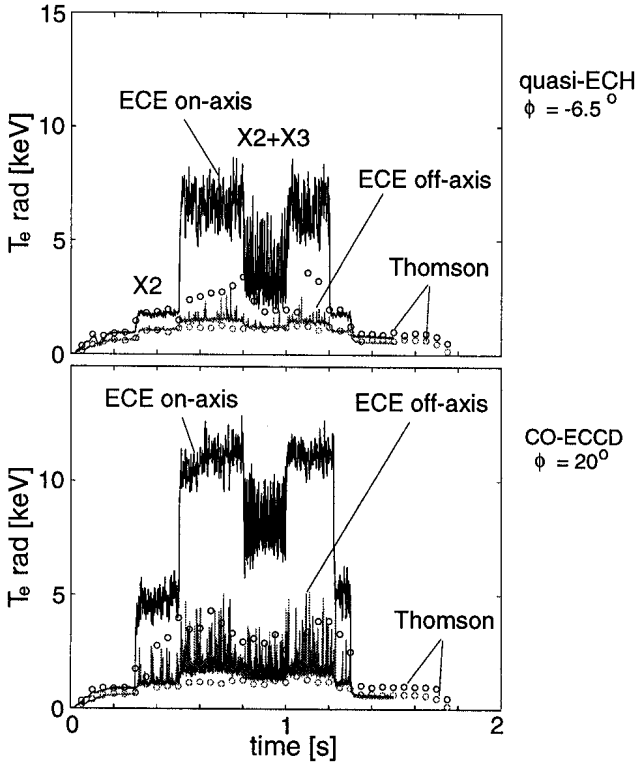

FIG. 5. Time traces of the high field-side ECE radiometer: quasi-ECH at $\phi = -6.5^o$ (top) and CO-ECCD at $\phi = 20^o$ (bottom). In both figures, two radiometer channels are shown: a on-axis view ($R = 0.88m$, black trace) and an off axis view (R= 0.75m, grey trace). All radiometer signals have been calibrated against the Thomson scattering diagnostic (circles) during the ohmic phase ($t < 0.3s$). $P_{X2} \approx P_{X3} = 0.47MW$.

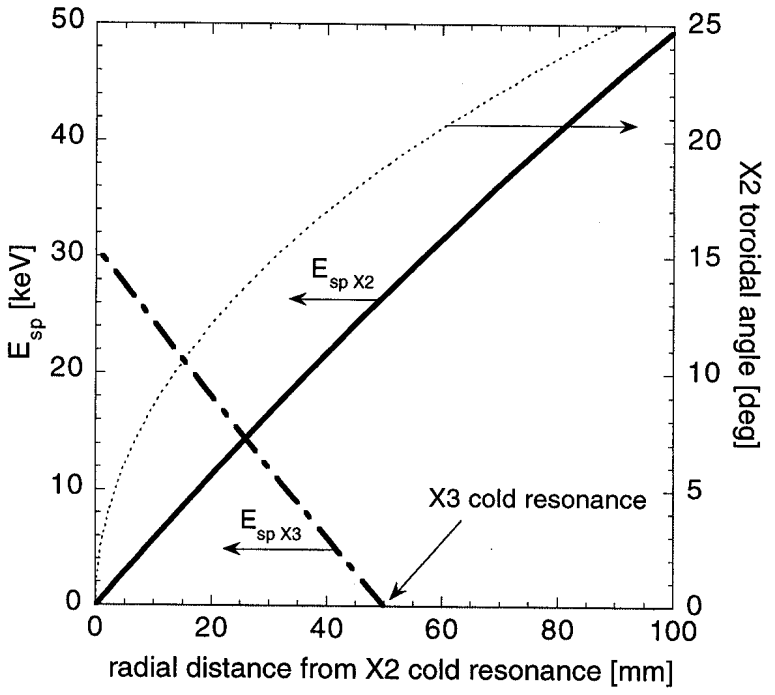

FIG. 6. Single particle resonance energies (left y-axis, E_{sp}) for X2, E_{spX2} (solid line), and X3, E_{spX3} (dash-dotted line), waves versus radial distance from the X2 cold resonance going towards the low-field side. For an oblique incidence with toroidal angle ϕ, the dashed line indicates the radial position at which the X2 wave starts to interact with electrons having a kinetic energy E_{spX2}.